Inorganic Chemistry

pubs.acs.org/IC Article

Crystalline Structure and Thermal Stability of an Unknown ZIF-L300 Phase

Jiajun Zhong, Lixiong Qian, Hao Wang, Yunpeng Liu, Lei Yao, Yuecheng Lai, Jianxin Song, Xin Wang, Yikun Li, Xueqing Xing, Guang Mo, Yuanyuan Tan, Zhongjun Chen, and Zhonghua Wu*

Cite This: *Inorg. Chem.* 2023, 62, 4385−4391 Read Online

ACCESS | Metrics & More | Article Recommendations | Supporting Information

ABSTRACT: In recent years, the synthesis, crystalline structure, and applications of zeolite imidazole frameworks (ZIFs) have attracted extensive attention. Since the ZIF-L phase was synthesized, a new phase was observed during the heating process, but its crystal structure is unknown. The unknown new phase, which was named ZIF-L300 in this study, was confirmed again. In this study, the X-ray powder diffraction technique and Rietveld refinement were used to solve the crystalline structure of the unknown ZIF-L300 phase. The results demonstrate that ZIF-L300 has the same chemical formula ($ZnC_8N_4H_{10}$) as in ZIF-8 and belongs to a hexagonal structure with a space group of $P6_1$. The lattice parameters have been determined as follows: $a = b = 8.708(7)$ Å, $c = 24.195(19)$ Å, $\alpha = \beta = 90°$, and $\gamma = 120°$. The X-ray absorption fine structure (XAFS) technique was also used to extract the local atomic structures. The in situ X-ray diffraction (XRD) technique was used to monitor the structural evolution of the as-prepared ZIF-L in a temperature range from room temperature to 600 °C. The results show that the sample experiences a change process from the initial ZIF-L orthorhombic phase (<210 °C), to the ZIF-L300 hexagonal phase (~300 °C), then to an amorphous phase (~390 °C), and finally to a zincite ZnO phase (>420 °C). These sorts of structural information are helpful to the application of ZIF materials and enrich the knowledge of the thermal stability of ZIF materials.

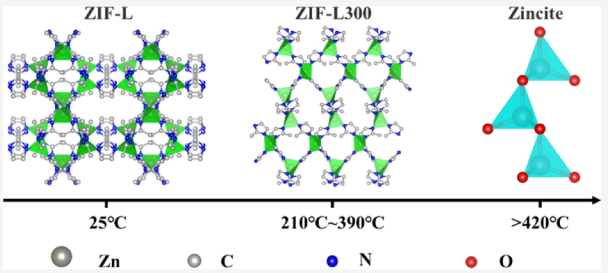

1. INTRODUCTION

Zeolitic imidazolate frameworks (ZIFs) are highly ordered porous materials, being an important branch of MOF materials. So far, many ZIF materials have been reported, among which ZIF-8,[1] ZIF-67,[2] and ZIF-L[3] are typical. ZIF-L is another popular ZIF series material after ZIF-8, which was first reported by Chen et al..[3] Its large two-dimensional surface and large aperture cavity have attracted the attention of researchers. Since its discovery, ZIF-L has been widely used for large surface loads and gas adsorption. It has been found that ZIF-L had a 2D layered network structure, and the large cavity in its crystal unit cell causes an average micropore volume of 0.066 $cm^3\ g^{-1}$. Even so the crystal structure of ZIF-L still showed a good thermal stability at 150 °C in air or a good pressure stability up to 6.3 GPa. The structural characteristics of 2D layered networks make ZIF-L an excellent membrane material. The ZIF-L membrane exhibited a higher CO_2 adsorption capacity or a superior adsorption selectivity for CO_2/CH_4,[3] CO_2/H_2,[4] and other gases.[5,6] It also exhibited a superior permeability and selectivity for water treatment and organic dehydration from ethanol/water,[7] oil/water,[8] and other aqueous phases.[9,10] As a better adsorbent than other ZIFs, ZIF-L was used to quickly remove inorganic salts,[11] dyes[12] from water, or CO_2[13] from air. In addition, when ZIF-L was burned at 600 °C, the as-formed N-doped carbon layered nanosheets would be an excellent doping carrier material.[14−17]

Since ZIF-L was reported for the first time, there have been some research studies about the ZIF-L pyrolysis process. The early studies[3,18] claim that the pyrolysis process of ZIF-L in air can be generally divided into two stages, i.e., the decomposition stage of the ZIF-L framework and the formation stage of ZnO. It is almost a consensus among researchers that the first stage of ZIF-L pyrolysis is described as the loss of guest water molecules and weakly linked 2-methylimidazole molecules (abbreviated as Hmim). However, few studies[19] have been conducted on an unknown new crystalline phase that appeared around 300 °C during pyrolysis. Such an unknown new phase is considered a priori to be a different Zn-Hmim complex, there has been no detailed structural report until now. It is well known that the ZIF consists of inorganic metal ions and imidazolate ligands. Each metal ion (M) is located at the center of the N_4 tetrahedral environments. All of

Received: January 14, 2023
Published: March 1, 2023

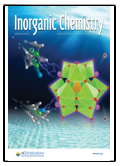

https://doi.org/10.1021/acs.inorgchem.3c00160
Inorg. Chem. 2023, 62, 4385−4391

these M−N_4 tetrahedral environments are bridged together by imidazolate ligands. The appearance of such an unknown new phase around 300 °C means that the original ZIF-L crystal phase must have undergone a phase transition or thermal decomposition. At present, there is still a gap in the research on the change of the structure of the pyrolysis process, but ZIF-L has been used as an effective catalyst support,[20−22] and the pyrolysis process is a necessary process for the synthesis of such catalysts. If the pyrolysis process is proved, it will be helpful for the regulated synthesis of catalysts with ZIF-L as the precursor carrier. Therefore, the determination of the crystalline structure of this unknown new phase is very important and necessary to understand the pyrolysis process and thermal stability of ZIF-L.

In this work, a mixed solution method was used to synthesize the ZIF-L material. Temperature-dependent XRD measurements were performed for clarifying the possible pyrolysis process or phase change of the as-prepared ZIL-L. The unknown new phase is named ZIF-L300, its crystal structure is determined, and the structural change of the ZIF-L phase with temperature is discussed in this study.

2. EXPERIMENTS

2.1. ZIF-L Synthesis. First, 1.314 g of dimethyl imidazole was dissolved in 15 mL of deionized water to form solution A, and 1.190 g of zinc nitrate hydrate was dissolved in 30 mL of deionized water to form solution B. Then, solution A was poured into solution B to form mixed solution and let to stand still at room temperature for 72 h. Third, the mixed solution was centrifuged with deionized water three times and alcohol one time for collecting the precipitation product. Fourth, the collected precipitate was placed into the evaporation dish for evaporating the residual solvent. Finally, the precipitate was dried in a vacuum drying oven at 60 °C for 12 h. As the synthesized product, the white powder was collected and labeled as ZIF-L.

2.2. ZIF-L300 Preparation. The synthesized white powder was put into an alumina crucible. Then, the alumina crucible containing the white powder was heated in a tube furnace, and the tube furnace was exposed to air, and the heating rate was 10 °C/min. The white powder was heated from room temperature to 300 °C. After holding on 300 °C for 1 h, the powder sample was naturally cooled to room temperature. In this heating process, the white powder in the alumina crucible had transferred into brown. Finally, the collected brown powder was ground evenly and labeled as ZIF-L300 for further use.

2.3. XRD and XAFS Measurements. XRD patterns of ZIF-L white powder and ZIF-L300 brown powder were acquired at Beamline 4B9A of the Beijing Synchrotron Radiation Facility (BSRF). The incident X-ray wavelength was 1.5403 Å, which was obtained by monochromatizing the incident X-ray white light with the Si (111) double crystal monochromator. The energy resolution ($\Delta E/E$) was about 3×10^{-4}. The scanning step of the 2θ angle was set to 0.02°. The counting time for each data point was set to 5 s. The collected range of 2θ angles was from 7.5° to 80°. The distance between the detector and the sample was about 700 mm. The opening of the front slit in front of the powder sample was 3×0.5 mm^2, and the opening of the receiving slit in front of the detector was 7×1 mm^2. A heating furnace purchased from Anton Paar was used to realize the in situ temperature-dependent XRD measurements for ZIF-L.

After the ZIF-L powder was homogeneously mixed with BN powder, the mixed powder was pressed into a pill and used for XAFS measurements. In such a pill sample, the content of ZIF-L powder was adjusted to have an absorption thickness ($\Delta\mu d$) of about 1 at the Zn−K edge. In situ XAFS measurements of Zn K-edge were performed for this ZIF-L powder sample at Beamline 4B9A of the BSRF. The storage ring was run at 2.5 GeV with an electron current of about 150 mA. A Si (111) double-crystal monochromator was used to monochromatize the incident X-ray energy with an energy resolution ($\Delta E/E$) of about 3×10^{-4}. A heating furnace (HTC-TXAS) purchased from Beijing Scistar Technology Co, Ltd. was used to change the sample temperature.

3. DISCUSSION

3.1. Determination of the ZIF-L300 Crystal Structure. First, the white powder of ZIF-L has been heat-treated at 300 °C to a brown powder and is labeled as ZIF-L300. The XRD pattern of ZIF-L300 was collected at room temperature and is shown in Figure 1. For comparison, the room-temperature

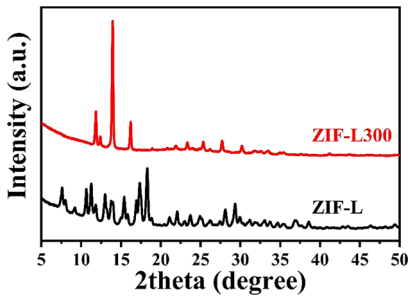

Figure 1. Room-temperature XRD patterns of the ZIF-L (bottom) and the ZIF-L300 (top) heat-treated at 300 °C for 1 h. The incident X-ray wavelength was 1.54 Å.

XRD pattern of ZIF-L was also collected and is shown in Figure 1. The completely different XRD patterns between ZIF-L300 and ZIF-L demonstrate that ZIF-L300 has a different crystal structure from the one of ZIF-L. Although the same XRD pattern[19] as that of ZIF-L300 has been observed, its corresponding crystal structure has not been reported. Therefore, the crystal phase with the same XRD pattern as that of ZIF-L300 is still attributed to an unknown new phase. To solve the crystal structure of ZIF-L300, the XRD pattern of ZIF-L300 needs first to be indexed by EXPO2014 via the program N-TREOR09[23] and Dicvol06.[24] After removing the scattering background generated automatically by software, a total of 17 stronger peaks with their 2θ positions at 11.74, 12.30, 13.84, 16.10, 18.82, 21.84, 23.22, 25.22, 27.58, 30.06, 31.64, 32.54, 33.32, 34.80, 35.22, 37.46, and 41.06° were selected. The intensities and positions of these 17 diffraction peaks were used to judge and search for the initial candidate unit cells.

By restricting the unit-cell volume within a range from 0 to 4000 $Å^3$, the candidate unit-cell parameters searched by using N-TREOR09 and Dicvol06 are shown in Table 1 and satisfy the indexing requirements. Furthermore, these candidate unit cells with M20 factor greater than 10 are generally believed to be more reliable. Thus, cases 4 and 5 in Table 1 can be excluded first. When selecting a candidate unit cell, in principle, the larger the M20 factor, the better. When M20 factors are close, the higher the unit-cell symmetry, the better. After considering the extinction rule, the space group of $P6_1$ of the hexagonal unit cell with $a = b = 8.700$ Å, $c = 24.181$ Å, $\alpha = \beta = 90°$, and $\gamma = 120°$ matches best.

Before further data treatment, the type and number of atoms in the unit cell as well as the chemical formula are necessary. It is well known that the chemical formula of the ZIF-L molecule is $Zn(mim)_2(Hmim)_{0.5}(H_2O)_{1.5}$ ($ZnC_{10}H_{16}N_5O_{1.5}$), and its molar mass is 295.65 g/mol. In this study, after three groups of 100.6, 100.3, and 101.1 mg of ZIF-L white powder were calcined at 300 °C for 1 h, the obtained brown powder (ZIF-

https://doi.org/10.1021/acs.inorgchem.3c00160
Inorg. Chem. 2023, 62, 4385−4391

Table 1. Initial Candidate Unit Cells Screened Out by Using N-TREOR09 (the First Five) or by Using Dicvol06 (the Last Two)

case	prog	a (Å)	b (Å)	c (Å)	α (°)	β (°)	γ (°)	volume (Å^3)	M20	symmetry
1	N	8.699	8.699	24.159	90	90	120	1583.07	28	$P6_3$ _ _
2	N	8.710	8.710	24.198	90	90	120	1589.78	23	$P6_3$ _ _
3	N	8.693	8.693	24.094	90	90	120	1576.97	26	$P6_3$ _ _
4	N	8.728	15.105	8.564	90	109.91	90	1061.65	9	C1 _ 1
5	N	8.686	15.029	8.553	90	109.85	90	1050.23	10	$P1$ a 1
6	D	24.172	7.539	4.350	90	90	90	792.67	30.6	orthogonal
7	D	8.700	8.700	24.181	90	90	120	1585.13	27.7	hexagonal

L300) weighed respectively 78.1, 75.2, and 79.2 mg. The mass loss was about 22.5, 25.1, and 21.9 mg, which was about average 23% of the original mass. In each ZIF-L molecule, 0.5 Hmim radicals and 1.5 H_2O molecules are connected by relatively weak hydrogen bonds that break more easily than other bonds. If 0.5 Hmim radical and 1.5 H_2O molecules were ablated from each ZIF-L molecule during heat treatment, the remaining portion can be represented with the chemical formula as Zn(mim)$_2$ ($ZnC_8N_4H_{10}$). The calculated molar weight of Zn(mim)$_2$ is 227.58 g/mol. This means that the weight loss would be 68.07 g/mol when Zn-(mim)$_2$(Hmim)$_{0.5}$(H_2O)$_{1.5}$ was calcined into Zn(mim)$_2$. In other words, the relative weight loss would be 23%. We notice that this relative weight loss is close to the measured weight loss (23%). The errors of the three experiments are within 2%, which is mainly due to the difference in the mass lost during the transfer process. In addition, element analysis by scanning electron microscopy (SEM) and energy dispersion spectroscopy (EDS) also indicates that the element composition of Zn:C:N in the unknown new phase was close to 1:8:4 (Figure S1). Thus, the chemical formula of the unknown new phase (ZIF-L300) can be assumed to be Zn(mim)$_2$. Two mim radical fragments and one Zn atom were used to optimize their configurations in a unit cell by using EXPO2014.

Furthermore, it was reported that ZIF-L[3] was an orthorhombic system with space group *Cmca*. Its unit-cell parameters a = 24.1191(5) Å, b = 17.0604(3) Å, and c = 19.7398(4) Å. Based on these crystallographic parameters, it can be calculated that each Zn is coordinated by four nitrogen atoms to form a Zn−N_4 tetrahedron with Zn−N bond length of 1.99 Å in the ZIF-L phase. In this work, XAFS experiments were performed for the unknown new phase (ZIF-L300). From the analysis results in Table 2, it can be found that each

Table 2. EXAFS Fitting Parameters of the ZIF-L and ZIF-L300 Acquired with Software Artemis[25a]

sample	atom-pair	N	R (Å)	σ^2 (10^{-3} Å^2)	ΔE (eV)
ZIF-L-feff	Zn−N	4	1.98		
ZIF-L	Zn−N	4.0(8)	1.99(1)	4.3(17)	6.5(26)
ZIF-L300	Zn−N	4.0(5)	2.00(1)	4.4(11)	6.5(18)

[a]The structural parameters of ZIF-L,[3] as references and marked as ZIF-L-feff, are also given.

Zn is still coordinated by four nitrogen atoms in the ZIF-L300 phase; thus a preliminary structure of the ZIF-L300 phase can be obtained after the simulated annealing method. The preliminary results confirm that the Zn atom is indeed coordinated by four Hmim radicals. There are six molecules of Zn(mim)$_2$ in a unit cell (Z = 6).

Next, GSAS[26,27] software was used to refine the crystal structure of the unknown new phase. The XRD pattern of ZIF-L300 was collected with an incident X-ray wavelength of 1.5403 Å at room temperature (298 K), as shown in Figure 2.

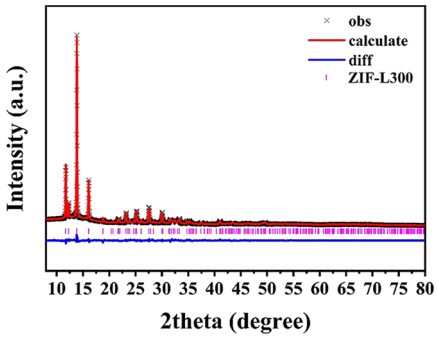

Figure 2. Rietveld refinement for the XRD pattern of ZIF-L300 samples. The black X symbols represent the observed values, the red solid line represents the calculated values, the blue solid line represents the residual values, and the pink tick marks represent the peak positions of Bragg reflections. The observed XRD pattern was collected at room temperature at a wavelength of 1.5403 Å.

The pseudo-Voigt function with symmetric correction was selected as the peak function. In the refinement process, dimethyl imidazole molecules were treated as a rigid body. The relative atomic positions in the rigid body were unchanged, but as a whole, the position and orientation of the rigid body in the unit cell were refined. After refinements, the crystal structure of ZIF-L300 was finally determined with R_{wp} = 0.049, R_p = 0.038, χ^2 = 1.36, and R-factor = 0.09. The best refined XRD pattern was compared and shown in Figure 2. The obtained refined unit-cell parameters are listed in Table 3.

Finally, the refined crystal structure of ZIF-L300 is shown in Figure 3, where three unit cells are projected on the *bc* plane and are parallelly arranged along the *b*-axis direction as shown in Figure 3a, and a 3 × 3 unit-cell array is projected on the *ab* plane as shown in Figure 3b. For clarity, all hydrogen atoms are not shown in Figure 3. Obviously, ZIF-L300 is still a framework material that consists of Zn-(mim)$_4$ tetrahedra. In the Zn-(mim)$_4$ tetrahedra, Zn is connected with four Hmim radicals through the N atom on the five-membered ring of Hmim, forming actually a Zn−N_4 tetrahedron. In each unit cell of ZIF-L300, there are six Zn atoms and 12 Hmim radicals, Z = 6. Although in both ZIF-L and ZIF-L300, Hmim was always bridging to two adjacent Zn-(mim)$_4$ tetrahedra through the two N atoms in the five-membered ring of Hmim, ZIF-L300 has a distinctly different structural characteristic as compared with the structure of ZIF-L. In the unit cell of ZIF-L300 with space group of $P6_1$, there is only one equivalent crystallo-

https://doi.org/10.1021/acs.inorgchem.3c00160
Inorg. Chem. 2023, 62, 4385−4391

Table 3. Refined Crystallographic Parameters for the Crystal Structure of ZIF-L300

parameter	value
chemical formula	$Zn(C_4N_2H_5)_2$
M_w (g/mol)	227.58
space group	$P6_1$ (No. 169)
a (Å)	8.708(7)
b (Å)	8.708(7)
c (Å)	24.195(19)
α (°)	90.0
β (°)	90.0
γ (°)	120.0
V (Å^3)	1589.0(32)
Z	6
D_x (g/cm^3)	1.428
X-ray wavelength (Å)	1.5403
T (K)	298(2)
scan type	ω, 2ω

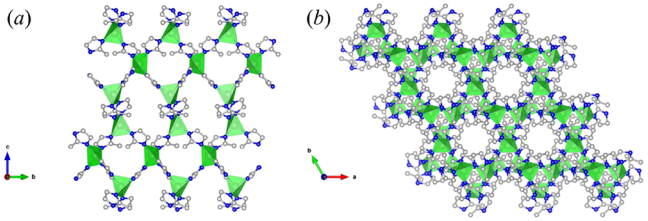

Figure 3. ZIF-L300 unit-cell projections on the bc plane where three unit cells are in parallel arrangement along the b-axis direction (a), and on the ab plane where 3 × 3 unit-cell arrays are shown (b). In this figure, the green tetrahedra represent the Zn−N_4 tetrahedral structure, the blue balls represent the N atoms, and the gray balls represent the C atoms. For clarity, all H atoms are not shown in this figure.

graphic site of Zn(II) cations, the six Zn(II) cations are all located at the 6a site, and each of the 12 imidazole units is bonded to two Zn(II) cations. While in the unit cell[3] of ZIF-L with space group of Cmca, there are 24 molecules (Z = 24) and two types of different crystallographic sites of Zn(II) cations. Sixteen of the 24 Zn(II) cations are located at the 16 g site and the other eight Zn(II) cations are located at the 8e site. Partial imidazole units are bonded to two Zn(II) cations, partial imidazole units are bonded to one Zn(II) cations, and partial imidazole units and water molecules are only filled in the framework.

Interestingly, ZIF-L300 shares the same chemical formula $Zn(mim)_2$ as ZIF-8 but has a different crystal structure. It is well known that ZIF-8 is a cubic phase[1] with space group of I-43m. In the unit cell of ZIF-8, there are 12 molecules $Zn(mim)_2$, Z = 12. There is only one equivalent crystallographic site (12d) for the 12 Zn(II) cations in the unit cell. Similarly, each imidazole unit in the unit cell of ZIF-8 is also bonded to two Zn(II) cations, the same as in ZIF-L300. Finally, the refined atomic coordinates of $Zn(mim)_2$ molecules in the unit cell of hexagonal ZIF-L300 are listed in Table 4.

From the above discussion, it is clear that the ZIF-L300 is an intermediate product during the pyrolysis process of ZIF-L around 300 °C. When the initial ZIF-L phase $Zn(mim)_2(Hmim)_{0.5}(H_2O)_{1.5}$ was heated to high temperature, the weak bonded water molecules and the monodentate Hmim radical were dissociated from the ZIF-L molecules. The remaining pyrolysis product was just the ZIF-L300 phase,

Table 4. Rietveld Refined Atomic Coordinates in the Hexagonal Unit Cell of ZIF-L300 with Space Group of $P6_1$ and Lattice Parameters (a = b = 8.708(7) Å, c = 24.195(19) Å, α = β = 90°, γ = 120°)

atom	occu.	X	Y	Z	100*Uiso
C1	1	0.5432(1)	0.1965(4)	0.7728(1)	0.094(4)
C2	1	0.7170(4)	0.3148(18)	0.7451(5)	0.094(4)
N1	1	0.4284(11)	0.0299(5)	0.7584(3)	0.094(4)
N2	1	0.4786(13)	0.2406(12)	0.8161(1)	0.094(4)
C3	1	0.2868(4)	−0.0379(11)	0.7942(6)	0.094(4)
C4	1	0.3187(12)	0.0969(22)	0.8311(3)	0.094(4)
H1	1	0.1841(8)	−0.1543(14)	0.7948(9)	0.132(4)
H2	1	0.2413(20)	0.0869(33)	0.8609(4)	0.132(4)
H3	1	0.8115(1)	0.3593(17)	0.7722(7)	0.132(4)
H4	1	0.7172(2)	0.4061(20)	0.7221(6)	0.132(4)
H5	1	0.7384(15)	0.2441(28)	0.7186(4)	0.132(4)
C5	1	0.8677(3)	0.4793(1)	0.9282(1)	0.094(4)
C6	1	0.8405(15)	0.2984(3)	0.9164(5)	0.094(4)
N3	1	0.9825(1)	0.5942(11)	0.9646(0)	0.094(4)
N4	1	0.7812(5)	0.5511(12)	0.9041(2)	0.094(4)
C7	1	0.9734(12)	0.7474(4)	0.9630(4)	0.094(4)
C8	1	0.8447(14)	0.7199(10)	0.9244(4)	0.094(4)
H6	1	1.0408(18)	0.8545(9)	0.9840(5)	0.132(4)
H7	1	0.8102(21)	0.8053(17)	0.9146(7)	0.132(4)
H8	1	0.7153(17)	0.2116(2)	0.9184(5)	0.132(4)
H9	1	0.9153(19)	0.2681(13)	0.9381(6)	0.132(4)
H10	1	0.8801(17)	0.2985(0)	0.8789(5)	0.132(4)
Zn1	1	0.5636(9)	0.4524(9)	0.8602(4)	0.050(2)

which has been confirmed to have a chemical formula of $Zn(mim)_2$. To clarify further the thermal stability and the possible pyrolysis process, the in situ XRD study will be performed for the as-prepared ZIF-L product in the next section.

3.2. Thermal Stability of ZIF-L. The in situ XRD technique was used to monitor the structural change of ZIF-L crystals with temperature. The obtained XRD patterns of ZIF-L at different temperatures are shown in Figure 4a. From room temperature (25 °C) to high temperature (600 °C), an obvious change of crystal phase is visible from the XRD patterns. When the sample temperature was at 25 °C, its XRD pattern can be attributed to the ZIF-L crystal phase.

When the sample temperature rose to 210 °C, its XRD pattern was very similar to the XRD pattern of the ZIF-L crystal phase, illustrating that the ZIF-L orthorhombic phase is still the dominant phase of the sample when its heat-treated temperature is below than 210 °C. When the sample temperature increased from 240 to 360 °C, their XRD patterns were very similar but different from the one of ZIF-L at room temperature, behaving as the number decrease of diffraction peaks. In this temperature range, the main crystal phase can be attributed to an unknown new phase and was labeled as ZIF-L300, in which the diffraction peak at 13.8° is a fingerprint of the ZIF-L300 phase. When the sample temperature was at 390 °C, there were no diffraction peaks in its XRD pattern. This means that the sample was already an amorphous phase. With the temperature increasing from 420 to 600 °C, the sample showed obviously different XRD patterns, which can be attributed to the crystal structure of ZnO. In fact, the characteristic peak of ZIF-L300 also appeared at 13.8° of the XRD pattern at 210 °C, implying that ZIF-L and ZIF-L300 phases coexisted at 210 °C. These results demonstrate that the

https://doi.org/10.1021/acs.inorgchem.3c00160
Inorg. Chem. 2023, 62, 4385−4391

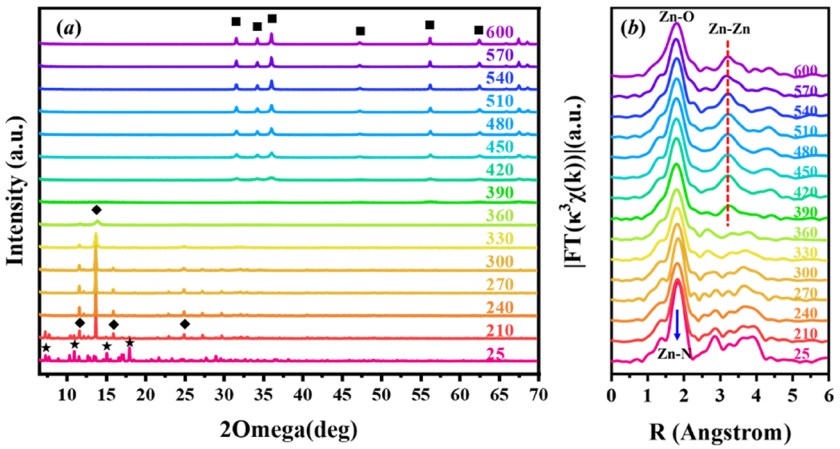

Figure 4. (a) Temperature-dependent XRD patterns obtained with in situ XRD measurements. A structure change process from the initial ZIF-L phase (asterisks) to the unknown new phase ZIF-L300 (rhombuses), then to the amorphous phase (without peaks), and finally to the ZnO phase (squares) can be determined. (b) Temperature-dependent Fourier transform spectra obtained from the in situ XAFS measurements of the Zn K-edge of the as-prepared ZIF-L product. Noteworthy change of the second coordination peaks can be directly observed, being consistent with the changes of temperature-dependent XRD patterns.

initial ZIF-L crystal phase experienced a thermal decomposition and had a structural change from the ZIF-L phase to ZIF-L300 change at about 210 °C. However, the complete disappearance of diffraction peaks at 390 °C means that the pyrolysis of the newly formed ZIF-L300 phase happened and an amorphous structure had been formed. It was the pyrolysis of the ZIF-L300 phase that results in the subsequent formation of ZnO, as confirmed by the higher temperature XRD patterns.

The temperature-dependent Fourier transform spectra of k^3-weight Zn K-edge XAFS spectra are shown in Figure 4b. As indicated by the XRD pattern, the room-temperature (25 °C) sample is the ZIF-L phase, in which the Zn central atom is coordinated by four N neighbors at a Zn−N bond length of 1.99 Å to form a Zn−N_4 tetrahedron. In the ZIF-L phase, the Zn−N_4 tetrahedra are connected together by the bridging imidazolate ligands. Obviously, the four N coordination atoms contribute to the first coordination peak located at about 1.8 Å, while the imidazolate ligands contribute to the higher coordination shells in a range from 2 to 4 Å. When the temperature rose to 210 °C, the XRD pattern tells us that an unknown new phase (ZIF-L300) appeared in the product. Although the first coordination peak is located still at about 1.8 Å, the higher coordination peaks at 2−4 Å are more disordered due to the coexistence of two phases. When ZIF-L300 becomes the dominant phase in the sample, it seems that the first coordination peak located at about 1.8 Å was still similar to the one in the ZIF-L phase, but the higher coordination peaks at 2−4 Å showed a larger change. This result implies that the ZIF-L300 new phase has a similar nearest near-neighbor structure, but a different second near-neighbor structure with the ZIF-L phase. When the temperature reached 390 °C, the sample can be attributed to an amorphous phase from the XRD pattern without visible diffraction peaks; however, an obvious coordination peak located at about 3.2 Å suggests that the sample still has a somewhat medium-range order. Evidently, XAFS is more sensitive to the structural change as compared with XRD. With the further increase of temperature from 420 to 600 °C, the first-shell coordination peak located around 1.8 Å widened, and the high-shell coordination peak located at about 3.2 Å became more prominent. In fact, the sample had been pyrolyzed and ZnO was formed above 390 °C. The nearest near-neighbor Zn−N_4 coordination structure in ZIF-L or ZIF-L300 phases has been transferred into the Zn−O coordination structure in ZnO. The first coordination peaks located at about 1.8 Å were isolated by the Fourier filter for further XAFS fitting. The XAFS fitting results are shown in Table 5. It can be seen that the nearest near-neighbor coordination structures around the central Zn atoms are almost the same for ZIF-L and ZIF-L300 phases; all four N atoms are around Zn with a Zn−N bond-length of 2.00 or 1.99 Å. However, for the amorphous sample at 390 °C, the Zn−O coordination has entered the nearest near-neighbor, resulting in structural disorder and the coexistence of Zn−N and Zn−O atom-pairs. The coordination numbers of Zn−N and Zn−O in the sample reveal that it includes about 34% of the ZIF-L300 phase and 66% of ZnO phase, being a two-phase coexistent sample.

Table 5. Temperature-Dependent XAFS Fitting Parameters for the In Situ XAFS Spectra, Which Were Obtained with Software Artemis[25a]

sample	atom-pair	N	R (Å)	σ^2 (10^{-3} Å^2)	ΔE (eV)
ZIF-L	Zn−N	4	1.98		
25 °C	Zn−N	4.0(3)	2.00(1)	4.1	5.6(16)
210 °C	Zn−N	4.0(3)	2.00(1)	6.1	4.5(16)
240 °C	Zn−N	4.0(2)	2.00(1)	6.6	3.9(15)
270 °C	Zn−N	4.0(3)	2.00(1)	6.7	4.3(17)
300 °C	Zn−N	4.0(3)	1.99(1)	7.1	4.3(15)
330 °C	Zn−N	4.0(3)	1.99(1)	7.7	3.7(19)
360 °C	Zn−N	4.0(3)	1.98(1)	8.1	3.7(23)
390 °C	Zn−N (34%)	4.0(2)	1.98(1)	9.7	2.1(5)
	Zn−O (66%)	4.0(2)	1.95(1)	9.7	2.1(5)
420 °C	Zn−O	4.0(2)	1.96(1)	9.9	2.0(10)
450 °C	Zn−O	4.0(2)	1.96(1)	10.0	2.3(10)
510 °C	Zn−O	4.0(1)	1.96(1)	10.1	2.2(10)
540 °C	Zn−O	4.0(2)	1.96(1)	10.2	1.8(12)
570 °C	Zn−O	4.0(2)	1.95(1)	10.5	1.4(14)
600 °C	Zn−O	4.0(1)	1.96(1)	11.1	2.0(5)
ZnO	Zn−O	4	1.96		

[a]As references, the near-neighbor structures around central Zn atoms in ZIF-L[3] and ZnO[28] are also given.

https://doi.org/10.1021/acs.inorgchem.3c00160
Inorg. Chem. 2023, 62, 4385−4391

When the heat-treated temperature was above 390 °C, the $Zn-N_4$ near-neighbor structure of the ZIF-L phase had transformed completely to the $Zn-O_4$ near-neighbor structure of the ZnO phase, and the high-shell coordination peaks located around 3.2 Å were the contribution of Zn-Zn atom-pairs, as shown in Figure 4b. The Zn *K*-edge fitting curves in *R*-space of k^3-weight EXAFS spectra are shown in the Supporting Information as Figures S2−S15.

From the discussion above and TGA results (Figure S16, SI), we have known that the as-prepared ZIF-L experiences the following changes as it was calcined in air. First, ZIF-L is stable below 210 °C. With the temperature increasing from 210 to 360 °C, the ZIF-L phase rapidly disappeared. The ZIF-L300 phase experienced a change from gradual enhancement to disappearance. The thermal decomposition of ZIF-L phase can be described as eq 1.

$$Zn(mim)_2(Hmin)_{0.5}(H_2O)_{1.5} \triangleq Zn(mim)_2 + 0.5Hmim\uparrow + 1.5H_2O\uparrow \quad (1)$$

From 360 to 420 °C, the pyrolysis of the ZIF-L300 phase is accompanied by the further dissociation of Hmim, and the sample experienced a change from complete disappearance of ZIF-L300 phase, to an amorphous phase, then to the formation of a zincite ZnO phase with hexagonal symmetry and the space group of $P6_3mc$. When the temperature further increases from 420 to 600 °C, the amorphous phase will be completely oxidized to ZnO. The further thermal decomposition oxidation reaction of the ZIF-L300 phase can be described as eq 2

$$2Zn(mim)_2 + O_2 \triangleq 2ZnO + 2mim\uparrow \quad (2)$$

4. CONCLUSIONS

In this paper, the thermal stability and the pyrolysis product of ZIF-L were studied by using the in situ X-ray powder diffraction technique and XAFS technique. The conclusions can be summarized as follows.

1) An unknown new phase appearing in the pyrolysis of ZIF-L around 300 °C is confirmed again and named ZIF-L300, and now the crystallographic structure of ZIF-L300 has been determined to be a hexagonal structure with a space group of $P6_1$. The chemical formula of ZIF-L300 is $ZnC_8N_4H_{10}$. Its unit-cell parameters have been refined: $a = b = 8.708(7)$ Å, $c = 24.195(19)$ Å. $\alpha = \beta = 90°$, $\gamma = 120°$. Each unit cell contains six $Zn(mim)_2$ parts of ZIF-L300.
2) During the heating process of ZIF-L from room temperature to 600 °C, the structural evolution from ZIF-L, to ZIF-L300, then to an amorphous phase, and finally to ZnO has been clarified. Below 210 °C, the orthorhombic ZIF-L phase is stable. From 210 to 360 °C, accompanying the decomposition of water and partial Hmim radicals from ZIF-L, the crystalline phase ZIF-L300 is from appearing to disappearing. At about 390 °C, the sample is completely transferred to the amorphous phase. From 420 to 600 °C, the amorphous phase can be oxidized to a complete ZnO zincite phase.

■ ASSOCIATED CONTENT

Supporting Information

The Supporting Information is available free of charge at https://pubs.acs.org/doi/10.1021/acs.inorgchem.3c00160.

SEM-EDS analysis of ZIF-L300; *R*-space fitting curves of Zn K-edge EXAFS spectra with k^3-weight; the test samples were the as-prepared products, which were heat-treated at different temperatures for 1 h, respectively; the heat-treated temperatures are shown as the name of the sample; and TGA result of ZIF-L from 25 to 600 °C (PDF)

Accession Codes

CCDC 2208597 contains the supplementary crystallographic data for this paper. These data can be obtained free of charge via www.ccdc.cam.ac.uk/data_request/cif, or by emailing data_request@ccdc.cam.ac.uk, or by contacting The Cambridge Crystallographic Data Centre, 12 Union Road, Cambridge CB2 1EZ, UK; fax: +44 1223 336033.

■ AUTHOR INFORMATION

Corresponding Author

Zhonghua Wu − *Institute of High Energy of Physics, Chinese Academy of Sciences, Beijing 100049, China; University of Chinese Academy of Sciences, Chinese Academy of Sciences, Beijing 100049, China;* orcid.org/0000-0002-8036-022X; Email: wuzh@ihep.ac.cn

Authors

Jiajun Zhong − *Institute of High Energy of Physics, Chinese Academy of Sciences, Beijing 100049, China; University of Chinese Academy of Sciences, Chinese Academy of Sciences, Beijing 100049, China*

Lixiong Qian − *School of Materials Science and Engineering, Northeastern University, Shenyang 110819, PR China*

Hao Wang − *Institute of High Energy of Physics, Chinese Academy of Sciences, Beijing 100049, China; University of Chinese Academy of Sciences, Chinese Academy of Sciences, Beijing 100049, China*

Yunpeng Liu − *Institute of High Energy of Physics, Chinese Academy of Sciences, Beijing 100049, China;* orcid.org/0000-0002-3783-0054

Lei Yao − *Institute of High Energy of Physics, Chinese Academy of Sciences, Beijing 100049, China*

Yuecheng Lai − *Institute of High Energy of Physics, Chinese Academy of Sciences, Beijing 100049, China; University of Chinese Academy of Sciences, Chinese Academy of Sciences, Beijing 100049, China*

Jianxin Song − *Institute of High Energy of Physics, Chinese Academy of Sciences, Beijing 100049, China; School of Environmental and Material Engineering, Yantai University, Yantai 264005, China*

Xin Wang − *Institute of High Energy of Physics, Chinese Academy of Sciences, Beijing 100049, China; College of Materials Science and Engineering, Qiqihar University, Qiqihar 161006, China*

Yikun Li − *Institute of High Energy of Physics, Chinese Academy of Sciences, Beijing 100049, China; School of Chemical Engineering and Light Industry, Guangdong University of Technology, Guangdong 510006, China*

Xueqing Xing − *Institute of High Energy of Physics, Chinese Academy of Sciences, Beijing 100049, China;* orcid.org/0000-0002-1052-6319

Guang Mo − *Institute of High Energy of Physics, Chinese Academy of Sciences, Beijing 100049, China*

Yuanyuan Tan − *State Key Laboratory of Nonlinear Mechanics, Institute of Mechanics, Chinese Academy of Sciences, Beijing 100190, P R China*

https://doi.org/10.1021/acs.inorgchem.3c00160
Inorg. Chem. 2023, 62, 4385−4391

Zhongjun Chen − *Institute of High Energy of Physics, Chinese Academy of Sciences, Beijing 100049, China*

Complete contact information is available at: https://pubs.acs.org/10.1021/acs.inorgchem.3c00160

Notes

The authors declare no competing financial interest.

■ ACKNOWLEDGMENTS

The XAFS measurements were carried out at the beamline 4B9A of Beijing Synchrotron Radiation Facility (BSRF). This work was supported by the National Key R&D Program of China (Grant Nos. 2022YFA1603802, 2017YFA0403000, and 2017YFA0403100).

■ REFERENCES

(1) Park, K. S.; Ni, Z.; Cote, A. P.; Choi, J. Y.; Huang, R.; Uribe-Romo, F. J.; Chae, H. K.; O'Keeffe, M.; Yaghi, O. M. Exceptional chemical and thermal stability of zeolitic imidazolate frameworks. *Proc. Natl. Acad. Sci. U. S. A.* **2006**, *103*, 10186−10191.

(2) Banerjee, R.; Phan, A.; Wang, B.; Knobler, C.; Furukawa, H.; O'Keeffe, M.; Yaghi, O. M. High-throughput synthesis of zeolitic imidazolate frameworks and application to CO_2 capture. *Science* **2008**, *319*, 939−943.

(3) Chen, R.; Yao, J.; Gu, Q.; Smeets, S.; Baerlocher, C.; Gu, H.; Zhu, D.; Morris, W.; Yaghi, O. M.; Wang, H. A two-dimensional zeolitic imidazolate framework with a cushion-shaped cavity for CO_2 adsorption. *Chem. Commun.* **2013**, *49*, 9500−9502.

(4) Kim, S.; Shamsaei, E.; Lin, X. C.; Hu, Y. X.; Simon, G. P.; Seong, J. G.; Kim, J. S.; Lee, W. H.; Lee, Y. M.; Wang, H. T. The enhanced hydrogen separation performance of mixed matrix membranes by incorporation of two-dimensional ZIF-L into polyimide containing hydroxyl group. *J. Membr. Sci.* **2018**, *549*, 260−266.

(5) Zhong, Z. X.; Yao, J. F.; Chen, R. Z.; Low, Z.; He, M.; Liu, J. Z.; Wang, H. T. Oriented two-dimensional zeolitic imidazolate framework-L membranes and their gas permeation properties. *J. Mater. Chem. A* **2015**, *3*, 15715−15722.

(6) Zhang, F.; Dou, J.; Zhang, H. Mixed Membranes Comprising Carboxymethyl Cellulose (as Capping Agent and Gas Barrier Matrix) and Nanoporous ZIF-L Nanosheets for Gas Separation Applications. *Polymers* **2018**, *10*, 1340.

(7) Mao, H.; Zhen, H. G.; Ahmad, A.; Li, S. H.; Liang, Y.; Ding, J. F.; Wu, Y.; Li, L. Z.; Zhao, Z. P. Highly selective and robust PDMS mixed matrix membranes by embedding two-dimensional ZIF-L for alcohol permselective pervaporation. *J. Membr. Sci.* **2019**, *582*, 307−321.

(8) Yuan, S. S.; Zhu, J. Y.; Li, Y.; Zhao, Y.; Li, J.; Van Puyvelde, P.; Van der Bruggen, B. Structure architecture of micro/nanoscale ZIF-L on a 3D printed membrane for a superhydrophobic and underwater superoleophobic surface. *J. Mater. Chem. A* **2019**, *7*, 2723−2729.

(9) Ting, H.; Chi, H.-Y.; Lam, C. H.; Chan, K.-Y.; Kang, D.-Y. High-permeance metal−organic framework-based membrane adsorber for the removal of dye molecules in aqueous phase. *Environ. Sci.: Nano* **2017**, *4*, 2205−2214.

(10) Liu, W.; Ban, Y. J.; Liu, J. Y.; Wang, Y. C.; Hu, Z. Y.; Wang, Y. H.; Li, Q. M.; Yang, W. S. ZIF-L based mixed matrix membranes for acetone-butanol-ethanol (ABE) recovery from diluted aqueous solution. *Sep. Purif. Technol.* **2021**, *276*, No. 119085.

(11) Huang, C.; Zhang, H. C.; Zheng, K. K.; Zhang, Z. H.; Jiang, Q. M.; Li, J. Two-dimensional hydrophilic ZIF-L as a highly-selective adsorbent for rapid phosphate removal from wastewater. *Sci. Total Environ.* **2021**, *785*, No. 147382.

(12) Chi, H.-Y.; Hung, S.-H.; Kan, M.-Y.; Lee, L.-W.; Lam, C. H.; Chen, J.-J.; Kang, D.-Y. Metal−organic frameworks for dye sorption: structure−property relationships and scalable deposition of the membrane adsorber. *CrystEngComm* **2018**, *20*, 5465−5474.

(13) Valencia, L.; Abdelhamid, H. N. Nanocellulose leaf-like zeolitic imidazolate framework (ZIF-L) foams for selective capture of carbon dioxide. *Carbohydr. Polym.* **2019**, *213*, 338−345.

(14) Chen, D.; Lu, R. H.; Pu, Z. H.; Zhu, J. W.; Li, H. W.; Liu, F.; Hu, S.; Luo, X.; Wu, J. S.; Zhao, Y.; Mu, S. C. Ru-doped 3D flower-like bimetallic phosphide with a climbing effect on overall water splitting. *Appl. Catal., B* **2020**, *279*, No. 119396.

(15) Li, X. D.; Zhang, W. D.; Cai, J. X.; Yan, H. J.; Cui, M. Q.; Wu, G. X.; Li, M. C. Hierarchical nanosheets constructed by integration of bimetallic sulfides into N-Doped carbon: Enhanced diffusion kinetics and cycling stability for sodium storage. *Nano Energy* **2019**, *62*, 239−249.

(16) Sang, X. X.; Wu, H. B.; Zang, N.; Che, H. L.; Liu, D. Y.; Nie, X. D.; Wang, D. W.; Ma, X. X.; Jin, W. Co_2P nanoparticle/multi-doped porous carbon nanosheets for the oxygen evolution reaction. *New J. Chem.* **2021**, *45*, 8769−8774.

(17) Tuan, D. D.; Liu, W. J.; Kwon, E.; Thanh, B. X.; Munagapati, V. S.; Wen, J. C.; Lisak, G.; Hu, C.; Lin, K. A. Ultrafine cobalt nanoparticle-embedded leaf-like hollow N-doped carbon as an enhanced catalyst for activating monopersulfate to degrade phenol. *J. Colloid Interface Sci.* **2022**, *606*, 929−940.

(18) Zhong, Z. X.; Yao, J. F.; Low, Z. X.; Chen, R. Z.; He, M.; Wang, H. T. Carbon composite membrane derived from a two-dimensional zeolitic imidazolate framework and its gas separation properties. *Carbon* **2014**, *72*, 242−249.

(19) Jiang, X.; Chen, J.; Lyu, F.; Cheng, C.; Zhong, Q.; Wang, X.; Mahsud, A.; Zhang, L.; Zhang, Q. In situ surface-confined fabrication of single atomic Fe-N_4 on N-doped carbon nanoleaves for oxygen reduction reaction. *J. Energy Chem.* **2021**, *59*, 482−491.

(20) Jiang, H.; Xue, S. L.; Liu, Y. F.; Xing, W. H.; Chen, R. Z. Temperature-dependent synthesis of Pd@ZIF-L catalysts via an assembly method. *Microporous Mesoporous Mater.* **2017**, *243*, 16−21.

(21) Huo, M.; Wang, B.; Zhang, C.; Ding, S.; Yuan, H.; Liang, Z.; Qi, J.; Chen, M.; Xu, Y.; Zhang, W.; Zheng, H.; Cao, R. 2D Metal-Organic Framework Derived CuCo Alloy Nanoparticles Encapsulated by Nitrogen-Doped Carbonaceous Nanoleaves for Efficient Bifunctional Oxygen Electrocatalyst and Zinc-Air Batteries. *Chemistry* **2019**, *25*, 12780−12788.

(22) Wang, F.; Xu, Y.; Wang, Y.; Liang, Z.; Zhang, R.; Wang, Y.; Zhang, H.; Zhang, W.; Cao, R.; Zheng, H. Space-confined construction of two-dimensional nitrogen-doped carbon with encapsulated bimetallic nanoparticles as oxygen electrocatalysts. *Chem. Commun.* **2021**, *57*, 8190−8193.

(23) Altomare, A.; Campi, G.; Cuocci, C.; Eriksson, L.; Giacovazzo, C.; Moliterni, A.; Rizzi, R.; Werner, P. E. Advances in powder diffraction pattern indexing: N-TREOR09. *J. Appl. Crystallogr.* **2009**, *42*, 768−775.

(24) Boultif, A.; Louer, D. Powder pattern indexing with the dichotomy method. *J. Appl. Crystallogr.* **2004**, *37*, 724−731.

(25) Ravel, B.; Newville, M. ATHENA, ARTEMIS, HEPHAESTUS: data analysis for X-ray absorption spectroscopy using IFEFFIT. *J. Synchrotron Radiat.* **2005**, *12*, 537−541.

(26) Toby, B. H. EXPGUI, a graphical user interface for GSAS. *J. Appl. Crystallogr.* **2001**, *34*, 210−213.

(27) Larson, A. C.; Von Dreele, R. B. *General Structure Analysis System (GSAS)*; Los Alamos National Laboratory Report; LAUR, 2000.

(28) Aminoff, G. XXIV. Über Lauephotogramme und Struktur von Zinkit. *Zeitschrift für Kristallographie-Crystalline Materials* **1921**, *56*, 495−505.